IEEE Photonics Journal
An IEEE Photonics Society Publication

Open Access

Compact Powell-Lens-Based Low-Coherence Correlation Interrogation System for Fiber-Optic Fabry-Perot Sensors

Volume 11, Number 4, August 2019

Zhibo Ma
Tongxin Guo
Tianyang Zhang
Wei Wang
Haibin Chen
Xiongxing Zhang
Weizheng Yuan

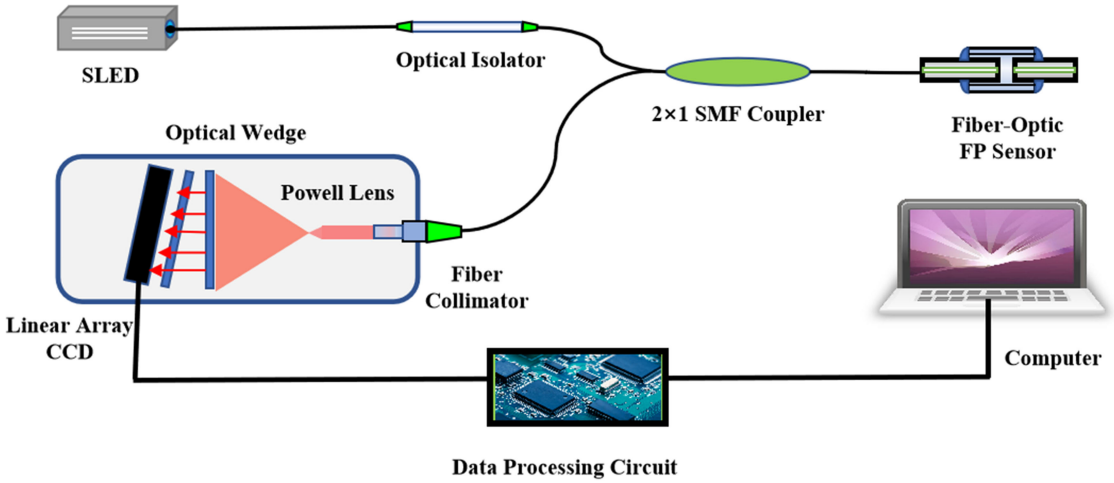

DOI: 10.1109/JPHOT.2019.2920432
1943-0655

IEEE photonics SOCIETY
IEEE

Compact Powell-Lens-Based Low-Coherence Correlation Interrogation System for Fiber-Optic Fabry-Perot Sensors

Zhibo Ma,[1,2] Tongxin Guo,[1,2] Tianyang Zhang,[3] Wei Wang,[3] Haibin Chen,[3] Xiongxing Zhang,[3] and Weizheng Yuan[1,2]

[1]Shaanxi Key Laboratory of MEMS/NEMS, Northwestern Polytechnical University, Xi'an 710072, China
[2]Key Laboratory of Micro/Nano Systems for Aerospace, Ministry of Education, Northwestern Polytechnical University, Xi'an 710072, China
[3]School of Optoelectronics Engineering, Xi'an Technological University, Xi'an 710021, China

DOI:10.1109/JPHOT.2019.2920432

Manuscript received April 15, 2019; revised May 27, 2019; accepted May 29, 2019. Date of publication June 3, 2019; date of current version July 2, 2019. This work was supported by the National Natural Science Foundation of China under Grant 51475384. Corresponding author: Wei Wang (email: wangwei@xatu.edu.cn).

Abstract: For the absolute cavity length interrogation of fiber-optic Fabry-Perot (FP) sensors, a low-coherence interferometer based on the Powell lens is proposed and demonstrated. The usage of a large-fan-angle Powell lens combined with a tiny fiber collimator for achieving a line-type beam and uniform beam-profile distribution improves the power adaptability of the system for different types of fiber-optic FP sensors. Furthermore, the system volume is considerably reduced, rendering it more compact than the conventional system using a cylindrical lens or mirrors.

Index Terms: Powell lens, Fabry-Perot cavity, low-coherence interferometer.

1. Introduction

Owing to advantages including high-sensitivity, compact size, light weight, chemical passivity, and resistance to electromagnetic interference, fiber-optic Fabry-Perot (FP) sensors have attracted significant attention from academic and industrial communities, and are extensively used in various areas[1]–[4]. Using heat or radiation resistant materials, such sapphires and SiCs, fiber-optic FP sensors demonstrate tremendous potential for application in extreme environments including high-temperature, high-pressure, high-radiation in aerospace, deep sea, and nuclear plants. [5]–[9].

For the practical application of fiber FP sensors, the interrogation technique plays a crucial role because it determines the resolution, accuracy, and operating rate of the entire sensing system. The interrogation methods for fiber FP sensors are mainly of two types: intensity interrogation and phase interrogation [10]–[13]. Although the signal detection and processing in intensity interrogation are relatively simple, disturbances from light-source fluctuation, optical-path losses, etc., are difficult to eliminate, and the sensing accuracy and system stability are relatively low. In

contrast, by extracting the sensing information through a phase discrimination method from the optical interference signal, phase interrogation methods can achieve high sensitivity.

As a type of phase interrogation method, correlation interrogation for fiber FP sensors includes advantages such as absolute measurement and large dynamic range. The correlation interrogation method can be classified into two categories: scanning correlation and nonscanning correlation. Nonscanning correlation interrogation is based on a low- coherence Fizeau interferometer, and the core correlation device is an air-gap or birefringent optical wedge. Compared to scanning correlation interrogation, nonscanning correlation interrogation has a high data-acquisition rate, high resolution, is robust against disturbance, etc.

To achieve the spatial correlation of an FP sensor with an optical wedge, the light transmitted in the fiber-optic path must be coupled into a beam propagating in free space. Generally, a CCD linear array, used as the signal receiver, has a length of several tens of millimeters; hence, the optical wedge should also have the same length or must be even longer. To completely utilize all the pixels of the CCD linear array and achieve a high-cavity-length interrogation resolution for the FP sensor, the beam radius of the coupled-out light should be expanded to cover all the pixels of the CCD linear array. Moreover, to completely utilize the light power, the light beam should not be expanded in the vertical direction.

To realize the above, a combination of a fiber collimator and a cylindrical lens or cylindrical mirror has been commonly proposed. The fiber collimator is used for expanding the light beam such that the beam radius covers all the pixels of the CCD linear array, while the cylindrical lens or mirror is used to refocus the light into a line-type beam [14]–[16]. However, to achieve a line-type-beam spot with a length of several centimeters, the size of the fiber collimator used is generally considerable, rendering the entire system relatively large.

In addition, it was proposed to directly couple-out the light from the fiber facet as divergent light, and focus this divergent light in a particular direction using a cylindrical lens or mirror to form the required line-type beam profile [17]– [20]. However, the numerical aperture (NA) of a single mode fiber (SMF) is generally less than 0.22, which renders the divergent angle relatively small. Only at a relatively long distance, the formed line-type beam can cover the entire range of the CCD linear array, resulting in an interrogation system that is not compact. Furthermore, the optical configuration introduces certain nonlinearity between the pixel position and the interrogated cavity length. Another problem in these types of systems is that the transverse intensity distribution of the beam is nonuniform and is commonly in a Gaussian form, which inevitably introduces certain obstacles and errors in the peak position determination of the correlation interferometric signal.

In order to address these issues, a Powell lens-based compact low-coherence correlation interrogation system for fiber-optic FP sensors is proposed, in this study. A novel compact line-type beam-shaping system consisting of a tiny optical fiber collimator and a Powell lens is proposed for a nonscanning correlation interrogating system. By combining a large-fan-angle Powell lens and a tiny fiber collimator to achieve a line-beam spot output and uniform beam-profile distribution, the power adaptability of the system for different types of fiber-optic FP sensors is effectively improved, while reducing the system volume considerably.

2. Interrogation Principle

There are many different types of intrinsic or extrinsic FP sensors, which can be fabricated using different materials through different methods; however, their basic structure and working mechanism are the same. A typical extrinsic FP sensor is shown in Fig. 1, which can be used for the sensing of various quantities, such as, strain/stress [21], curvature [22], displacement [23], temperature [24], etc. The sensor is composed of two vertically cut SMFs and a glass capillary. The two fiber ends are inserted into the glass capillary with a certain separation. The two facets of these SMFs are parallel to each other. When light is input through one of the SMFs, an interference effect is caused between the lights reflected by the two surfaces.The external physical or other types parameters affecting the cavity length can be measured by the length interrogation of the FP cavity. For FP sensors, there always exist an extra surface with undesirable reflection, to eliminate it, the surface

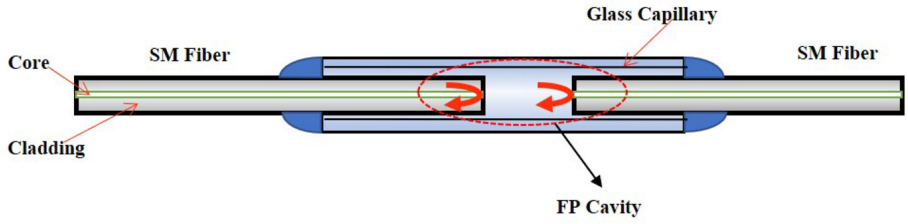

Fig. 1. Schematic of a fiber-FP sensor to be interrogated.

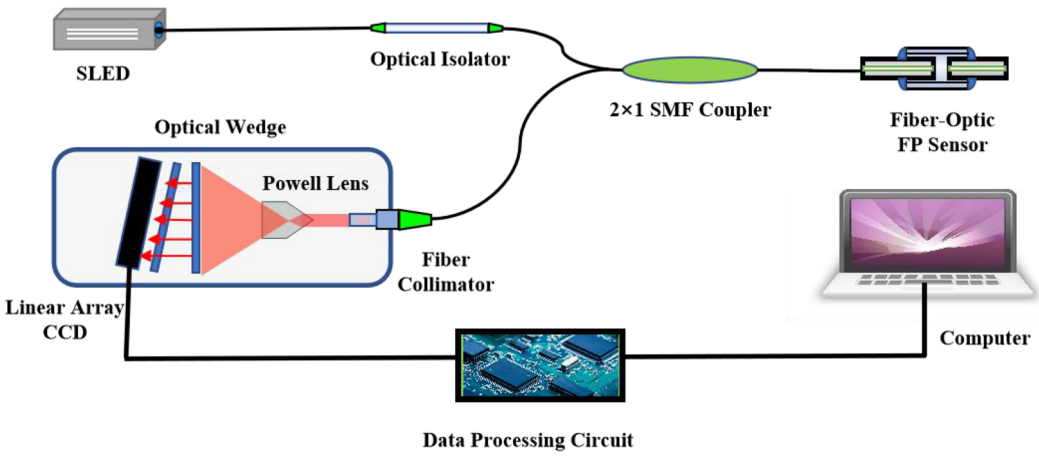

Fig. 2. Schematic diagram of a Powell lens-based low-coherence interrogation system.

can be roughen through a chemical or mechanical way, coated with an anti-reflection film, or tilted an angle of 8°.

The FP-sensor interrogation system, depicted in Fig. 2, is composed of a superluminescent light emitting diode (SLED), optical isolator, 2 × 1 SMF coupler, fiber collimator, Powell lens, optical wedge, CCD line array, data processing circuit, and a computer. The wideband light emitted by the SLED is coupled into the 2 × 1 SMF coupler after passing through the optical isolator, and is illuminated on the fiber-optic FP sensor. Part of the reflected light then is coupled back into the 2 × 1 SMF coupler. Half the light is coupled into the fiber collimator, and transformed into a collimated beam in free space. The Powell lens shapes the beam into a line-type beam, which then passes through the optical wedge and is received by the CCD linear array, which transforms the modulated light intensity distribution into an electric signal. The data processing circuit determines the maximum position for obtaining the cavity length of the fiber-optic FP sensor, which is then sent to the computer and displayed.

The core interrogation mechanism is based on the optical-length matching between the cavity length of the fiber-optic FP sensor and the optical wedge, both of which determine the modulated light intensity distribution illuminated on the CCD linear array.

If the SLED has a spectral density of $I_0(\lambda)$, for a single wavelength, λ, the reflected light of the fiber-optic FP sensor can be expressed as

$$I_{\mathrm{FPr}}(\lambda) = \frac{R_1 + R_2 - 2\sqrt{R_1 R_2}\cos\frac{4\pi nd}{\lambda}}{1 + R_1 R_2 - 2\sqrt{R_1 R_2}\cos\frac{4\pi nd}{\lambda}} I_0(\lambda), \tag{1}$$

where R_1 and R_2 are the reflection ratios of the two interfaces of the FP cavity, n is the refractive index of the material filled in the FP cavity, and d is the cavity length. For an air cavity, $n \approx 1$.

Half the reflected light is coupled into free space by the fiber collimator and Powell lens, and then passes through the optical wedge. If an air-gap optical wedge is used, the passing light for a wavelength, λ, can be expressed as

$$I_{\mathrm{Wt}}(\lambda, x) = \frac{(1-R_3)^2}{1+R_3^2-2R_3\cos\frac{4\pi L_p(x)}{\lambda}}\eta(x)\, I_{\mathrm{FPr}}(\lambda), \tag{2}$$

where the two inner surfaces of the air-gap optical wedge are supposed to have a reflection ratio of R_3; $L_p(x)$ is the separation of the two inner surfaces at a position, x; $\eta(x)$ is the intensity spatial distribution introduced by the fiber collimator and Powell lens. Suppose the inner separations of the air-gap optical wedge at the two ends are d_L and d_R ($d_L < d_R$), respectively,

$$L_p(x) = d_L + x\tan\theta, \tag{3}$$

where θ is the tilt angle of the air-gap optical wedge.

Considering all the wavelengths passing through the air-gap optical wedge, the modulated light intensity distribution illuminated on the CCD linear array can be expressed as

$$I_{\mathrm{Out}}(x) = \eta(x)\int_{\lambda_{\min}}^{\lambda_{\max}} \frac{R_1+R_2-2\sqrt{R_1R_2}\cos\frac{4\pi nd}{\lambda}}{1+R_1R_2-2\sqrt{R_1R_2}\cos\frac{4\pi nd}{\lambda}}\cdot\frac{(1-R_3)^2}{1+R_3^2-2R_3\cos\frac{4\pi L_p}{\lambda}}\cdot I_0(\lambda)d\lambda, \tag{4}$$

where $\lambda_{\min} \sim \lambda_{\max}$ is the wavelength range of the SLED source.

The signal received by the linear array CCD can be considered as a cross correlation operation between the cavity length of the FP sensor and the optical wedge, and can be called a correlation interferometric signal. For a position, x_m, if

$$nd = L_p(x_m) \tag{5}$$

is satisfied, the peak of the correlation interferometric signal will be formed. Hence, using an algorithm to find the peak position, x_m, the cavity length of the fiber-optic FP sensor can be determined as follows:

$$d = \frac{d_L + x_m\tan\theta}{n}. \tag{6}$$

3. Design and Simulation of the Powell Lens-Based Beam Shaping System

In a nonscanning correlation interrogating system, different positions of the wedge correspond to different cavity lengths. To utilize the light power completely and realize maximal detection range, the light that passes through the optical wedge and illuminates the CCD linear array should have a line-type beam profile with an appropriate size. However, as the light output from the fiber facet is a divergent beam, a beam-shaping system is required.

A novel compact line-type beam-shaping system consisting of a tiny optical fiber collimator and a Powell lens is proposed for the nonscanning correlation interrogating system, as shown in Fig. 3, in this study.

The Powell lens is a special type of aspherical lens, which has a 2D aspherical optical surface that be expressed by

$$Z = \frac{cr^2}{1+\sqrt{1+(1+\mathrm{k})c^2r^2}}, \tag{7}$$

where k is the cone coefficient of the quadric surface, c is a curvature parameter, and r is a position in the radial direction with respect to the central axis of the Powell lens.

When light from a tiny collimator is incident on the front optical surface, it rapidly converges in one dimension, and is finally refracted through the rear surface to form a line-type beam with a fan angle, θ. The fan angle is determined by the length, d_2, cone coefficient, k, and curvature, c, of the Powell lens, and is related to the incident beam radius.

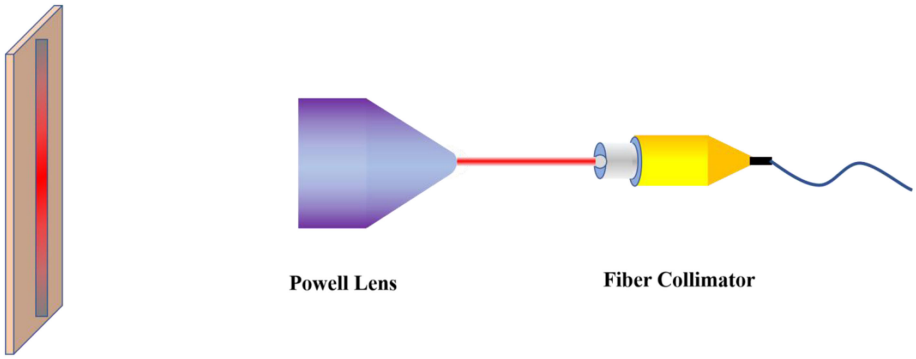

Fig. 3. Line-type profile beam-shaping system.

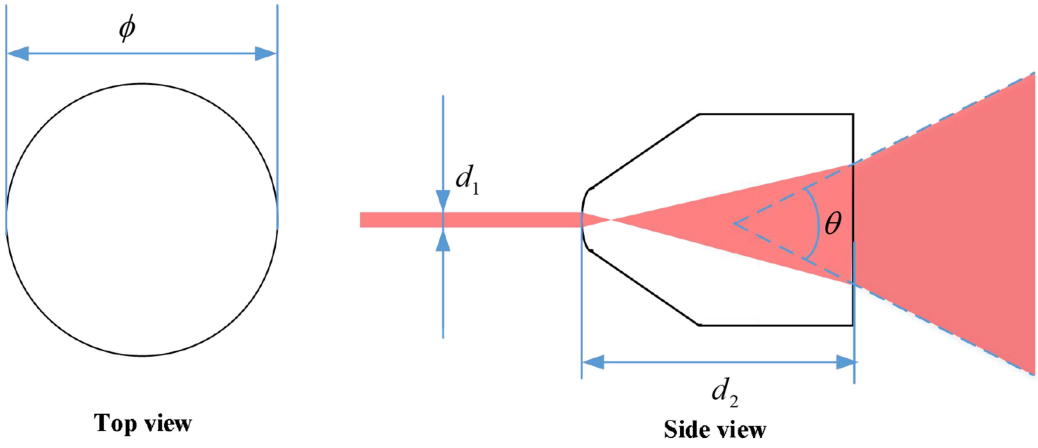

Fig. 4. Geometrical model of the Powell lens.

A geometrical model of the Powell lens was built in SolidWorks and imported into the optomechanical software, Tracepro, for simulation and optimization. The geometrical structure of the Powell lens built according to formula (7), is depicted in Fig. 4. The cone coefficient, k, was set to -1.6, the curvature, c, was set to 0.4, the diameter, ϕ, was set to 8 mm, the incident beam diameter was set to 0.4 mm according to the actual beam size of the fiber collimator used, and the length of the Powell lens, d_2, was set to 9 mm.

The three-dimensional model and simulation results of the Powell lens at a distance of 50 mm are shown in Fig. 5(a). The material used was BK7. Most of the incident light passed through the Powell lens and was converted into a line-type beam.

For comparison, a cylindrical lens was also simulated. The size of the cylindrical lens model was 35 mm $\times$ 35 mm $\times$ 2 mm (edge thickness), and its focal length was 50 mm. The same material, BK7, was used as in the Powell lens. The input light beam was a Gaussian beam with a beam waist diameter of 4 μm and half divergence angle of 6.35°, corresponding to the divergence angle of the light beam output from the SMF. The distance between the light source and cylindrical lens was set to 60 mm, as per the actual experiment setup. The intensity distribution of the light passing through the cylindrical lens was acquired at the focal plane of the cylindrical lens. The 3D cylindrical lens model and the simulation results are depicted in Fig. 5(b). Obviously, the beam size in the horizontal direction is relatively narrower than that of the Powell lens, and is considerably broader in the vertical direction.

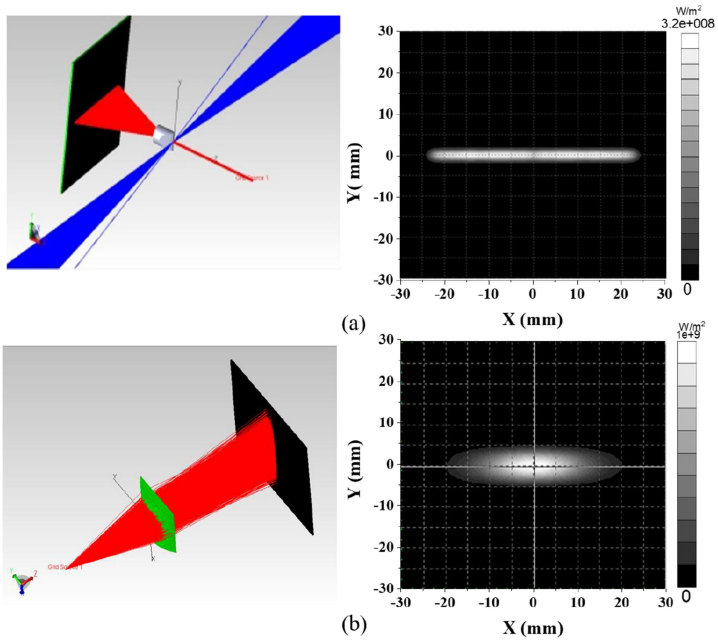

Fig. 5. 3D models and simulation results of the (a) Powell lens and (b) cylindrical lens, in which, the red rays represent strong passing light, and the blue rays represent relatively weak scattered light.

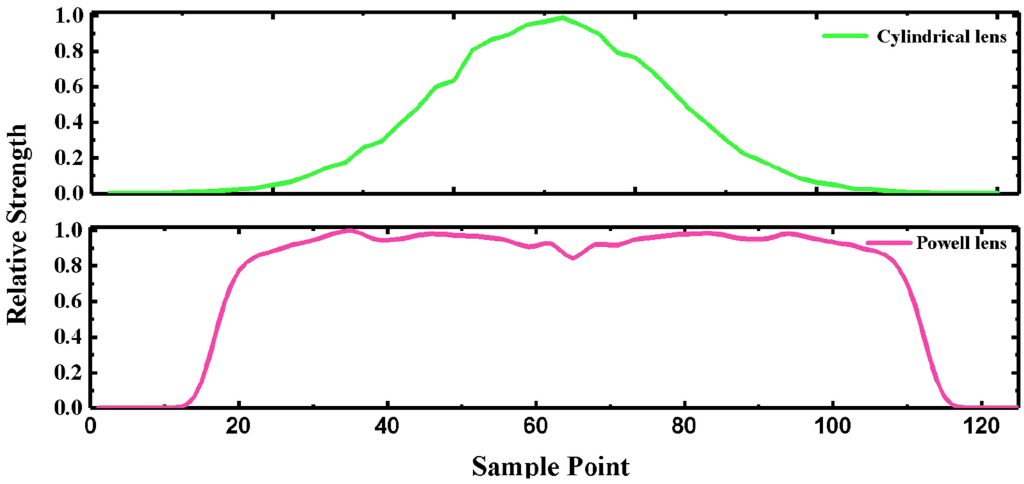

Fig. 6. Comparison of the relative intensity of the light output from a cylindrical lens and Powell lens.

Finally, the intensity distributions of the light output from the Powell lens and cylindrical lens were extracted, as shown in Fig. 6. The light intensity output from the cylindrical lens shows a Gaussian distribution, i.e., the center part of the beam is considerably brighter than the two sides, which may seriously affect the interrogation range of the low-coherence correlation interrogation system, if the power level of the reflected light from the fiber-optic FP sensor is too high, or too low. It is to be noted that the intensity distribution of the light output from the Powell lens was considerably more uniform and the intensity fluctuated only within a small range.

To evaluate the beam quality of the line-type beam, a light intensity coefficient, $Q = I_i/I_m$, was defined, where I_i is the light intensity at a certain point and I_m is the peak intensity. Furthermore, a uniformity coefficient was defined as $E = S_E/S$, where S_E is the range, when $Q \geq 0.5$ and S is the

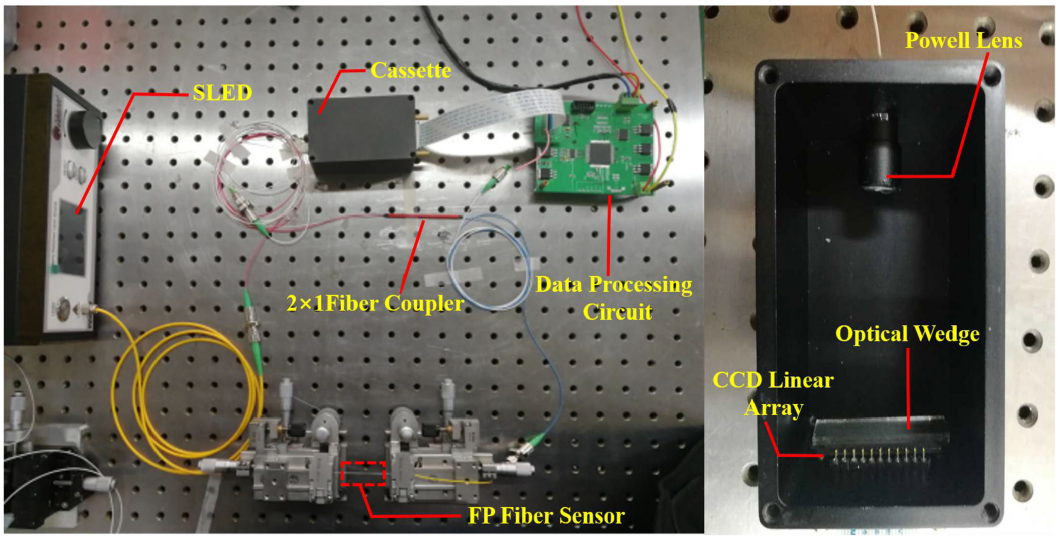

Fig. 7. Experimental setup of the Powell lens-based low-coherence correlation interrogation system. (a) Entire system. (b) Inner structure of the cassette.

total range of the beam spot. The uniformity coefficients of the Powell lens and cylindrical lens were 0.724 and 0.2344, respectively. The calculated uniformity coefficient of the cylindrical lens was less than that of the Powell lens.

When a Powell lens combined with a tiny fiber collimator is used, different from a cylindrical lens with stable focus, the CCD can be located according to the length of the detector window and fan angle of the Powell lens. Additionally, the size of the low-coherence correlation interrogation system can be reduced. Besides, the intensity distribution uniformity along the line direction of the reshaped beam profile can be considerably improved; this addresses the problem, where the edge signal of a linear array CCD cannot be detected because of the uneven distribution of the linear spot light generated by a cylindrical lens. The proposed system can maintain the available interrogation range for FP sensors even when the power level of the reflected light is relatively low. Thus, the combination of Powell lens with a tiny collimator is more suitable as a beam shaping system for a low-coherence correlation interrogation system.

4. Experiments and Discussions

A low-coherence correlation interrogation system based on the Powell lens was constructed; the experimental setup is shown in Fig. 7(a). The used SLED, in which an optical isolator was internally integrated, had a center wavelength of 850 nm and 3-dB spectral bandwidth of 58 nm. The 2×1 optical coupler (Thorlabs, TW850R5A2) was a wideband type, with a center working wavelength of 850 nm and minimal transmission range of $\pm$100 nm. A tiny fiber collimator and a Powell lens with a fan angle of 60° were used for coupling and emitting a liner-type beam to a distance of 50 mm, where a 3648 CCD linear array ((fabricated by Toshiba Semiconductor, TCD1304DG) was placed. The size of each pixel was 8 μm $\times$ 200 μm, the total photosensitive length was 29.2 mm, and the dynamic range was 300. It is to be noted that the output current signal of the CCD was inversely proportional to the light intensity. A handmade air-gap optical wedge with an air-gap thickness range of 55$-$105 μm, which was fabricated using two optical glass plates, was placed in front of the CCD linear array. Because of the imperfect of fabrication, and the spatial width of the correlation interferometric signal, the cavity length measuring range was shortened to 60$-$100 μm.

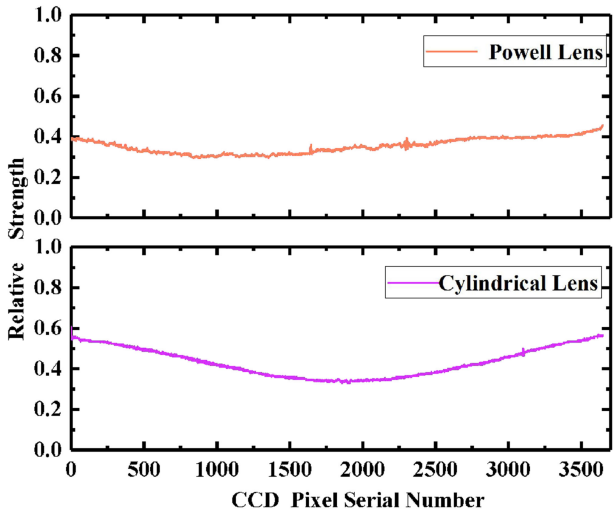

Fig. 8. Basal signals obtained from an SMF optical retroreflector with a uniform reflection ratio, connected to the low-coherence correlation interrogation system with beam-shaping based on a Powell lens and cylindrical lens, respectively.

The compact optical beam-shaping system composed of the fiber collimator, Powell lens, and air-gap optical wedge was assembled and sealed along with the CCD linear array in a metal cassette to avoid background-light disturbance on the CCD linear array and protect the optical-device surfaces from contamination due to dust. A self-designed signal processing circuit with an FPGA as the central processing chip was used for driving the CCD linear array, and, a peak positioning algorithm was used for realizing cavity length interrogation from the correlation interferometric signal obtained.

To verify the uniformity of the spatial line-type profile shaped by the compact optical beam-shaping system, an SMF optical retroreflector with a uniform reflection ratio was connected to the low-coherence correlation interrogation system shown in Fig. 7. As the FP cavity was not connected to the interrogation system, a correlation interferometric signal was not obtained. The output signal, referred to as the basal signal, only reflects the beam-shaping effect of the Powell lens. As observed in the top image of Fig. 8, the light distribution is relatively uniform on the CCD linear array; compared to that obtained from an optical beam-shaping system consisting of a cylindrical lens and a large-aperture fiber collimator (bottom image of Fig. 8), the uniformity of the light distribution in the beam profile is effectively improved.

Further, an extrinsic FP sensor with the same structure as that shown in Fig. 1 was connected to the Powell lens-based low-coherence correlation interrogation system. The fiber-optic FP sensor was constructed by inserting two vertically cut SMFs into a glass capillary with a certain separation. The diameter of the SMF core was 9 μm, and the outer diameter of the coating layer was 125 μm. The glass capillary had an inner diameter of 128 μm, outer diameter of 320 μm, and length of 30 mm.

The original correlation interferometric signal can be directly obtained from the CCD output, as shown in Fig. 9. However, noises and fake signals were present. To extract the peak position of the correlation interferometric signal of the fiber-optic FP sensor, a combined algorithm based on Fourier transform [25], bandpass filtering [26], and the gravity method [27] was used. In which, the correlation interferometric signal is firstly Fourier transformed into the frequency domain, and filtered out the low-frequency background signal and high-frequency noises by a bandpass filter; then, the signal is reversely transformed back to the spatial domain again, and the the envelope of the filtered correlation interferometric signal is fitted through a method of instantaneous effective value extraction; finally, the peak position of the envelope is found by gravity center searching in the signal range, and the corresponding innter separation of the optical wedge at the peak position is used to extract the cavity length of the fiber-optic FP sensor through formula (6).

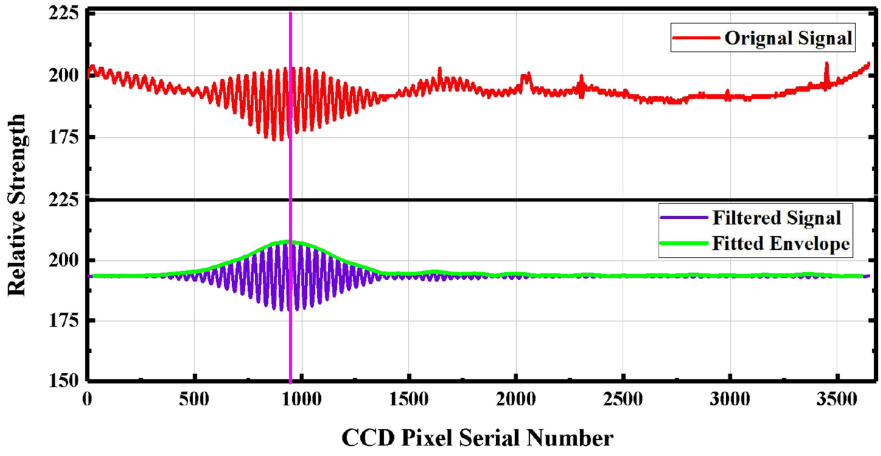

Fig. 9. Peak positioning of the correlation interferometric signal.

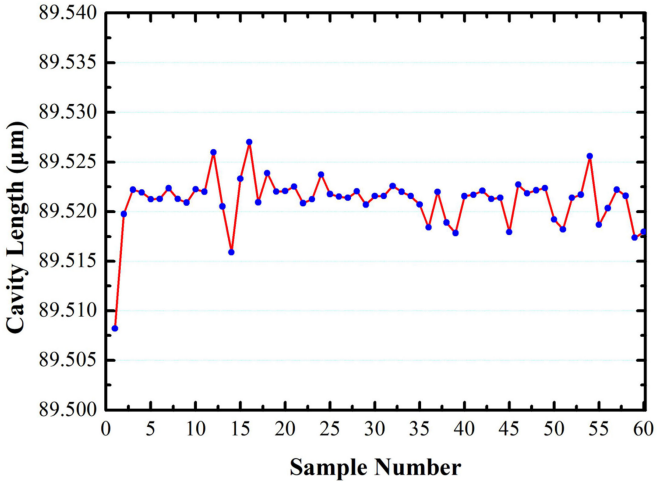

Fig. 10. Continuous cavity length interrogating results for a 89.521 μm fiber-optic FP sensor gotten by the Powell lens-based low-coherence correlation interrogation system.

The corresponding relationship between the cavity length and pixel point was determined through the system calibration process. Fiber-optic extrinsic FP sensors with cavity lengths of 60.003 μm, 65.002 μm, 69.998 μm, 74.999 μm, 80.001 μm, 84.998 μm, 90.002 μm, and 94.999 μm were fabricated and connected to the interrogation system, respectively. The peak positions for all the eight FP sensors were recorded. By a linear fitting method, the corresponding relationship between the cavity length and pixel point was obtained as

$$L_p = 0.0134779x + 55.95685\ \mu\text{m}. \tag{8}$$

The degree of fitting was $R^2 = 0.9999$, and the accuracy in the entire range of 60−100 μm reached a value of 0.04%.

To evaluate the resolution of the proposed Powell lens-based low-coherence correlation interrogation system, a fiber-optic FP sensor with a cavity length of 89.521 μm was connected to the interrogation system and continuously interrogated in a short time. As seen from Fig. 10, the continuous 60 times sampling of the interrogated results fluctuated in a very narrow range from 89.508 μm to 89.527 μm. A standard deviation about 2.537 nm can be calculated from these results, so the resolution is better than 2.54 nm.

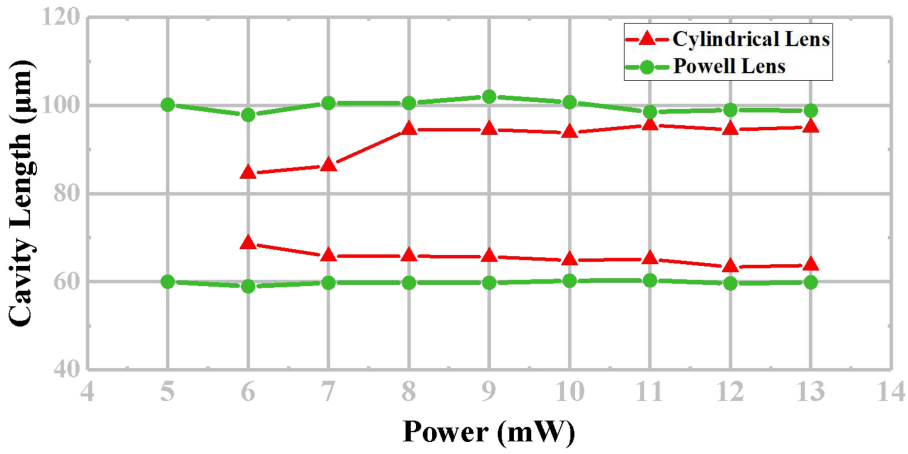

Fig. 11. Comparison of the interrogation range of the Powell-lens-based low coherence interrogation system under different light input power with that of the cylindrical lens-based interrogation system.

To investigate the power adaptability of the Powell lens-based low-coherence correlation interrogation system, experiments were conducted for the cavity-length interrogation of a cavity-length tunable FP sensor under different SLED output powers. The cavity-length tunable FP sensor was fixed to a pair of 5-axis precision translation stages for fine tuning the cavity length.

In the experiment, the cavity length was tuned within a wide range covering the separation range of the air-gap optical wedge, and the upper and lower limits of the cavity length that can be interrogated were determined for different fixed output powers of the SLED. As can be observed in Fig. 11, the cavity-length range that can be interrogated remained almost the same for the Powell lens system. The Powell lens-based interrogation system demonstrated a stable interrogation range, when the output power of the SLED was varied from 5−13 mW.

However, when the compact optical-beam shaping system was replaced by a cylindrical-based system, the cavity length range that could be interrogated decreased continuously with the decrease in the SLED output power. In particular, when the output power of the SLED was below 6 mW, the correlation interferometric signal disappeared, and the interrogation system failed to interrogate any cavity length. The reason is that, because of the Gaussian distribution of the light beam, the light intensity on the two sides of CCD linear array become too weak to be detected, as a result, when the cavity length of the FP sensor was in these ranges, it can't be interrogated. The lower the SLED output power, the shorter detectable range.

Obviously, the Powell lens-based low-coherence correlation interrogation system can maintain the available interrogation range for FP sensors for different power level of light. Thus, it can be concluded that the Powell lens-based interrogation system has better optical power adaptability. Moreover, this system has a wider interrogation range, compared the cylindrical lens-based one, under the same SLED output power.

Fiber-optic FP sensors can be fabricated using different types of materials, according to the different application environments. Different materials have different refractive indices, and different reflection ratios. Hence, the reflected light received by the CCD linear array will have different intensity levels. The proposed Powell-lens-based low-coherence interrogation system is advantages because it is more adaptable for the interrogation of different fiber-optic FP sensors, particularly when the reflected optical power is relatively low.

5. Conclusions

A large-fan-angle Powell lens combined with a tiny fiber collimator was proposed to realize a line-beam spot output and uniform beam-profile distribution for a low-coherence correlation interrogation system, for fiber-optic FP sensors. By optimizing the design of the optical system, the intensity

distribution of the line-type beam was made more uniform. Compared to an optical expanding and beam-shaping system based on a cylindrical lens or mirror, in the proposed system, the output beam does not require a fixed focus plane, rendering the tuning of the optical system more convenient; moreover, the interrogation performances, such as the interrogation range and optical power adaptability of the proposed system were improved. In addition, the system includes advantages such as compact size and low cost.

References

[1] Z. Huang, Y. Zhu, X. Chen, and A. Wang, "Intrinsic Fabry-Perot fiber sensor for temperature and strain measurements," *IEEE Photon. Technol. Lett.*, vol. 17, no. 11, pp. 2403–2405, Nov. 2005.

[2] T. W. Kao and H. F. Taylor, "High-sensitivity intrinsic fiber-optic Fabry-Perot pressure sensor," *Opt. Lett.*, vol. 21, no. 8, pp. 615–617, 1996.

[3] N. Furstenau, H. Horack, and W. Schmidt, "Extrinsic Fabry-Perot interferometer fiber-optic microphone," *IEEE Trans. Instrum. Meas.*, vol. 74, no. 1, pp. 138–142, Feb. 1998.

[4] K. D. Oh, J. Ranade, V. Arya, A. Wang, and R. O. Claus, "Optical fiber Fabry-Perot interferometric sensor for magnetic field measurement," *IEEE Photon. Technol. Lett.*, vol. 9, no. 6, pp. 797–799, Jun. 1997.

[5] H. Xiao, J. Deng, G. Pickrell, R. G. May, and A. Wang, "Single-crystal sapphire fiber-based strain sensor for high-temperature applications," *J. Lightw. Technol.*, vol. 21, no. 10, pp. 2276–2283, 2003.

[6] N. A. Riza and M. Sheikh, "Silicon carbide-based extreme environment hybrid design temperature sensor using optical pyrometry and laser interferometry," *IEEE Sensors J.*, vol. 10, no. 2, pp. 219–224, Feb. 2010.

[7] L. Cheng, A. J. Steckl, and J. Scofield, "SiC thin-film Fabry-Perot interferometer for fiber-optic temperature sensor," *IEEE Trans. Electron. Devices*, vol. 50, no. 10, pp. 2159–2164, Oct. 2003.

[8] N. Tuan-Khoa *et al.*, "Highly sensitive 4H-SiC pressure sensor at cryogenic and elevated temperatures," *Mater. Des.*, vol. 156, pp. 441–445, 2018.

[9] J. Yonggang, L. Jian, and Z. Zhiwen, "Fabrication of all-SiC fiber-optic pressure sensors for high-temperature applications," *Sensors*, vol. 16, no. 10, Oct. 17, 2016, Art. no. 1660.

[10] T. Yoshino, K. Kurosawa, K. Itoh, and T. Ose, "Fiber-optic Fabry-Perot interferometer and its sensor applications," *IEEE Trans. Microw. Theory Tech.*, vol. 30, no. 10, pp. 1612–1621, Oct. 1982.

[11] T. Guo, F. Li, and J. Chen, "Multi-wavelength phase-shifting interferometry for micro-structures measurement based on color image processing in white light interference," *Opt. Lasers Eng.*, vol. 82, pp. 41–47, 2016.

[12] D. V. Yurasov, A. Y. Luk Yanov, and P. V. Volkov, "Real-time measurement of substrate temperature in molecular beam epitaxy using low-coherence tandem interferometry," *J. Cryst. Growth*, vol. 413, pp. 42–45, 2015.

[13] C. Pang, M. Yu, and X. Zhang, "Multifunctional optical MEMS sensor platform with heterogeneous fiber optic Fabry-Pérot sensors for wireless sensor networks," *Sens. Actuators. A Phys.*, vol. 188, pp. 471–480, 2012.

[14] P. V. Volkov, A. V. Goryunov, and A. Y. Luk Yanov, "Fiber-optic temperature sensor based on low-coherence interferometry without scanning," *Optik*, vol. 124, no. 15, 2013.

[15] F. Cai, R. Tang, and S. Wang, "A compact line-detection spectrometer with a Powell lens," *Optik*, vol. 155, pp. 267–272, 2018.

[16] M. K. Chaudhury, T. Weaver, and C. Y. Hui, "Adhesive contact of cylindrical lens and a flat sheet," *J. Appl. Phys.*, vol. 80, no. 1, pp. 30–37, 1996.

[17] C. Ka and M. D. Morris, "Hyperspectral Raman microscopic imaging using Powell lens line illumination," *Appl. Spectrosc.*, vol. 52, no. 9, pp. 1145–1147, 1998.

[18] I. Powell, "Design of a laser beam line expander," *Appl. Opt.*, vol. 26, no. 17, pp. 3705–3709, 1987.

[19] Y. He, M. Xiaohui, and Z. Yonggang, "Beam shaping design for fiber-coupled laser-diode system based on a building block trapezoid prism," *Opt. Laser Technol.*, vol. 109, pp. 366–369, 2019.

[20] D. Adams, "Cylinder lenses for beam shaping," *Laser Technik J.*, vol. 15, no. 1, pp. 26–28, 2018.

[21] K. A. Murphy, M. F. Gunther, A. M. Vengsarkar, and R. O. Claus, "Quadrature phase-shifted, extrinsic Fabry-Perot optical fiber sensors," *Opt. Lett.*, vol. 16, no. 4, pp. 273–275, 1991.

[22] C. S. Monteiro, M. S. Ferreira, S. O. Silva, J. KobelkeKay, S. Bierlich, and O. Frazão, "Fiber Fabry-Perot interferometer for curvature sensing," *Photon. Sensors*, vol. 6, no. 4, pp. 339–344, 2016.

[23] N. A. Ushakov, L. B. Liokumovich, and A. A. Markvart, "Noise compensation in a Fabry-Perot-based displacement sensor operating at picometer-level resolution," *J. Phys. Conf. Ser.*, vol. 661, 2015, Art. no. 012047.

[24] A. Sakamoto and J. Nishii, "Fiber Fabry-Perot interferometer with precision glass-ceramic jacketing," *IEEE Photon. Technol. Lett.*, vol. 17, no. 7, pp. 1462–1464, Jul. 2005.

[25] K. Liu *et al.*., "An improved optical fiber remote sensing method based on polarized low-coherence interferometry," *IEEE Photon. J.*, vol. 10, no. 1, Feb. 2017, Art. no. 6800409.

[26] L. C. Dong, L. U. Huan, and and W. R. Li, "Adaptive main frequency bandpass filters used in Fourier transform profilometry," *Chin. J. Opt. Appl. Opt.*, vol. 3, no. 3, pp. 245–251, 2010.

[27] R. Dändliker, E. Zimmermann, and G. Frosio, "Electronically scanned white-light interferometry: A novel noise-resistant signal processing," *Opt. Lett.*, vol. 17, no. 9, pp. 679–681, 1992.